

Analysis of above-threshold ionization by “Wigner-distribution-like function” method

Li Guo¹, Mingqing Liu^{2,3}, Ronghua Lu¹, Shensheng Han¹ and Jing Chen^{2,4}

Review Article

Cite this article: Guo L, Liu MQ, Lu RH, Han SS, Chen J (2019). Analysis of above-threshold ionization by “Wigner-distribution-like function” method. *Laser and Particle Beams* **37**, 448–462. <https://doi.org/10.1017/S0263034619000569>

Received: 28 April 2019
Accepted: 21 July 2019
First published online: 18 September 2019

Key words:
above-threshold ionization; Wigner distribution

Author for correspondence:

Jing Chen, Institute of Applied Physics and Computational Mathematics, P. O. Box 8009, Beijing 100088, China and HEDPS, Center for Applied Physics and Technology, Collaborative Innovation Center of IFSA, Peking University, Beijing 100084, China, E-mail: chen_jing@iapcm.ac.cn

¹Key laboratory for Quantum Optics and Center for Cold Atom Physics, Shanghai Institute of Optics and Fine Mechanics, Chinese Academy of Sciences, Shanghai 201800, China; ²Institute of Applied Physics and Computational Mathematics, P. O. Box 8009, Beijing 100088, China; ³HEDPS, Center for Applied Physics and Technology, Collaborative Innovation Center of IFSA, Peking University, Beijing 100084, China and ⁴Center for Advanced Material Diagnostic Technology, College of Engineering Physics, Shenzhen Technology University, Shenzhen 518118, China

Abstract

Above-threshold ionization (ATI) is one of the most fundamental processes when atoms or molecules are subjected to intense laser fields. Analysis of ATI process in intense laser fields by a Wigner-distribution-like (WDL) function is reviewed in this paper. The WDL function is used to obtain various time-related distributions, such as time-energy distribution, ionization time distribution, and time-emission angle distribution and so on, of atoms in laser field pulses with different laser parameters. For the linearly polarized laser pulses, the time-energy distribution intuitively shows from a quantum point of view the relationship between the ionization moment and the final energy and clearly reveals the origin of interference structures in the photoelectron spectrum. In particular, for linearly polarized few-cycle laser pulses, all calculated distributions show the dependence of electron behavior on the ionization time, emission direction, and carrier-envelope phase (CEP). For elliptically polarized few-cycle pulses, we calculate the angular distribution, ionization time distribution, and time-emission distribution, which are compared with the semiclassical calculations. Analysis shows that the offset angle (difference between positions of the peaks in the angular distributions obtained by two methods) in the angular distributions does not correspond to the offset time (difference between positions of the peaks in the ionization time distributions obtained by two methods) in the ionization time distributions, which implies that the attosecond angular streaking technique based on this correspondence between the offset angle and time is in principle inaccurate. Furthermore, the offset time cannot be interpreted as tunneling time.

Introduction

Above-threshold ionization (ATI) is one of the most fundamental processes in strong field atomic physics, which was firstly observed by Agostini *et al.* (1979) and has been studied intensively since then (Kruit and Read, 1983; Lompré *et al.*, 1985; Offenberger *et al.*, 1995; Eslami and Basereh, 2013). When the laser field increases to be comparable to the ionic Coulomb field, electron in the bound state of the atom and molecule can absorb more photons than the minimum number required for ionization. In this ionization process, the perturbative theory is not valid and non-perturbative method has to be adopted (Keldysh, 1965; Faisal, 1973; Reiss, 1980). The corresponding physical process is known to be usually categorized into two distinct regimes: multiphoton ionization and tunneling ionization. These two regimes are distinguished by the Keldysh parameter $\gamma = \sqrt{I_p/2U_p}$ (I_p is the ionization potential and $U_p = E_0^2/4\omega^2$ denotes the ponderomotive energy where E_0 is the laser field peak strength and ω the laser frequency) (Keldysh, 1965). When γ is well above 1, the ionization process is in the multiphoton regime and the ATI energy spectrum consists of a series of regularly spaced narrow peaks, spacing by one photon energy (Agostini *et al.*, 1979), which comes from quantized energy of the photons in the laser field or, in a different point of view, can be attributed to interference between electrons freed from different optical cycles in the laser pulse (Arbó *et al.*, 2010). When γ is less than 1, the ionization process is in the tunneling regime. In the tunneling regime, the electron can be considered to tunnel through the barrier created by the superposition of the laser field and Coulomb potential and then classically moves in the external laser field. This is commonly known as the simpleman’s picture of the ATI process (Heuvell *et al.*, 1988), which comprises the picture to understand atomic and molecular dynamics in intense laser fields (Corkum, 1993; Becker *et al.*, 2002) and constitutes the foundation of attosecond measurement (Krausz and Ivanov, 2009).

Interference effect, as a universal phenomenon in quantum mechanics, was firstly investigated in ATI by Reed and Burnett (1991). They have attributed the subpeaks in each ATI peak, which is found by numerical solution of the one-dimensional time-dependent Schrödinger equation, to the interference between ionization amplitudes produced on the rising and falling

edges of the laser pulse. This structure is restudied by Wickenhauser *et al.* (2006) and is attributed to contributions of different laser cycles, which is called “inter-cycle” interference, to the final electron spectrum. Very recently, Della Picca *et al.* (2016) have concluded that electron emission amplitudes produced at different moments interfere with each other and produce the additional pattern that modulates the ATI peaks. Korneev *et al.* (2012) firstly reveal an obvious “carpet” pattern in the direction approximately perpendicular to the laser polarization in the velocity map of xenon in an 800 nm laser field. Based on the strong-field approximation (SFA) and saddle-point method, they have ascribed this pattern to the constructive and destructive interference of the long and short orbits of electrons ionized within one optical cycle, that is, “intra-cycle” interference, for a monochromatic field.

On the other hand, in semiclassical picture (namely Simpleman’s picture), the electron is ionized by the laser field via tunneling with exponential dependence of ionization probability on the electric field strength and then moves in the laser field, or in other words, there is a specific correspondence between the electron’s drift momentum and the ionization time ($\mathbf{P} = -\mathbf{A}(t)$, here \mathbf{P} is the electron momentum and $\mathbf{A}(t)$ is the vector potential of the laser field at the ionization time t) if the influence of the ionic potential is ignored.

Recently, an attosecond angular streaking technique, also dubbed as “attoclock” technique, has been developed to investigate the temporal dynamics of atoms and molecules in intense laser fields (Eckle *et al.*, 2008a; 2008b; Pfeiffer *et al.*, 2011; Wu *et al.*, 2012; Pfeiffer *et al.*, 2012a; Boge *et al.*, 2013; Landsman *et al.*, 2014). This technique, different from the conventional attosecond measurement which relies on attosecond pulses generated using high-order harmonic generation process and is very technically demanding, uses the rotating electric-field vector of an intense close-to-circularly polarized pulse to deflect photo-ionized electrons in the radial direction. Then the instant of ionization is mapped to the final angle of the momentum vector in the polarization plane according to the semiclassical picture. When a few-cycle pulse is applied, comparison between the peaks of the measured photoelectron angular distribution and the simple man’s prediction shows an offset angle which has caused much debate on its underlying mechanism (Eckle *et al.*, 2008b; Pfeiffer *et al.*, 2012a; Boge *et al.*, 2013; Ivanov and Kheifets, 2014; Landsman *et al.*, 2014). Ionic Coulomb potential, tunneling time delay and nonadiabatic effect have been proposed to explain this offset angle. By comparing the experimental data with the semiclassical calculation including the Coulomb potential, Eckle *et al.* (2008b) placed an intensity-averaged upper limit of 12 attoseconds on the tunneling delay time in strong-field ionization of a helium atom. Boge *et al.* (2013) have found that the nonadiabatic effect is unimportant. However, by solving a three-dimensional time-dependent Schrödinger equation, Ivanov and Kheifets (2014) gave an opposite view against the calculations using the semiclassical model (Boge *et al.*, 2013). Very recently, Torlina *et al.* (2015) have shown that the offset angle can be attributed to the Coulomb potential effect and confirm the zero tunneling time delay by theoretical calculation.

It is noteworthy that the principle of the attosecond streaking technique, viz., the angle of the final momentum vector corresponds to the instant of the tunneling ionization, is based on the semiclassical picture. Therefore, prior to consideration of the Coulomb potential and nonadiabatic effects and so on (Yudin and Ivanov, 2001; Eckle *et al.*, 2008b; Barth and Smirnova, 2011; Pfeiffer *et al.*, 2012b; Hofmann *et al.*, 2013; Wang *et al.*, 2014;

Klaiber *et al.*, 2015; Hofmann *et al.*, 2016), one needs to check rigorously the principle of the attoclock technique.

The Wigner distribution function (WDF) has been adopted as a powerful tool in time-frequency analysis and other aspects (Garg *et al.*, 1965). In strong-field atomic and molecular physics, the WDF has been used to investigate the time-frequency characteristic of high order harmonics generation process in atoms and molecules (Kim *et al.*, 2001; Chen *et al.*, 2006). Here we develop a Wigner-distribution-like (WDL) function based on the SFA theory (Reiss, 1980; Becker *et al.*, 2002) to study the time-energy distribution of photoelectron ionized from atoms by intense laser fields, which is difficult to be obtained in quantum theory.

In this paper, we give the detailed derivation of the WDL function (Guo *et al.*, 2010, 2012, 2016, 2017) in the section “Theory”. In the section “Results in linearly polarized laser fields”, we use the WDL function to analyze the dynamical behavior of the electrons ionized by linearly polarized multi-cycle and few-cycle laser pulses in parallel and perpendicular directions with respect to the polarization. The origin of the interference structures in the ATI spectrum is given. In the section “Results in elliptically and circularly polarized laser fields”, we use the WDL function to calculate the time-emission distribution, the ionization time distribution and the angular distribution for elliptically polarized few-cycle laser fields and also give the ionization time distribution for a circularly polarized laser field. By comparing with the corresponding results obtained by the semiclassical theory, we check the principle of the “attoclock” technique. Finally, we discuss the correspondence between the ionization time distributions obtained by the WDL function and semiclassical theory. In the section “Conclusions and outlook”, the conclusion is given.

Theory

The transition matrix element of the first term of the S-matrix expansion, that is, the SFA theory is in the form (Reiss, 1980):

$$S_{fi} = -i \int_{-\infty}^{\infty} dt \langle \chi_p(t) | V_I(t) | \varphi_i(t) \rangle. \tag{1}$$

Here, V_I is the interaction potential between the applied laser field and the photoelectron. V_I represents $\mathbf{p} \cdot \mathbf{A}(t) + A(t)^2/2$ in the velocity gauge while it is $\mathbf{r} \cdot \mathbf{E}(t)$ ($E(t)$ is the electric field amplitude) in the length gauge. $|\varphi_i(t)\rangle = |\varphi_0\rangle e^{iI_p t}$ is the atomic ground state and $|\chi_p(t)\rangle$ is the Volkov wavefunction with the final electron momentum \mathbf{p} , which has a form

$$|\chi_p(t)\rangle = \frac{1}{\sqrt{v}} \exp \left[i\mathbf{q} \cdot \mathbf{r} - i\frac{p^2}{2}t - i \int_{-\infty}^t \left[\mathbf{p} \cdot \mathbf{A}(\tau) + \frac{A(\tau)^2}{2} \right] d\tau \right], \tag{2}$$

where v is normalization volume. \mathbf{q} is equal to \mathbf{P} in the velocity gauge and $\mathbf{p} + \mathbf{A}(t)$ in the length gauge, respectively. Introducing Eq. (2) into Eq. (1), we obtain

$$\begin{aligned} S_{fi} &= \frac{-i}{\sqrt{v}} \int_{-\infty}^{\infty} dt \langle \mathbf{q} | V_I | \varphi_0 \rangle \\ &\quad \times \exp \left[i \int_{-\infty}^t \left[\mathbf{p} \cdot \mathbf{A}(\tau) + \frac{A(\tau)^2}{2} \right] d\tau + iI_p t + i\frac{p^2}{2}t \right] \\ &= \frac{1}{\sqrt{2\pi}} \int_{-\infty}^{\infty} dt S' e^{i(p^2/2)t}, \end{aligned} \tag{3}$$

where S' is given by

$$S' = \frac{-i\sqrt{2\pi}}{\sqrt{v}} \langle \mathbf{q} | V_I | \varphi_0 \rangle \exp \left[i \int_{-\infty}^t \left[\mathbf{p} \cdot \mathbf{A}(\tau) + \frac{A(\tau)^2}{2} \right] d\tau + i\mathbf{p}t \right] \quad (4)$$

It is noted that the expression of Fourier Transform has a form

$$F(\Omega) = \frac{1}{\sqrt{2\pi}} \int_{-\infty}^{\infty} F'(t) e^{i\Omega t} dt. \quad (5)$$

By comparing Eq. (3) with Eq. (5), one can find that S_{fi} is a Fourier-like transform of S' . So, we defined a WDL function in analog with Kim *et al.* (2001) to obtain the time-energy distribution of the photoionization process described by Eq. (1). The WDL function is defined as (Guo *et al.*, 2010, 2012)

$$f\left(t, \frac{p^2}{2}\right) = \frac{1}{\pi} \int_{-\infty}^{\infty} S'^*(t+t') S'(t-t') e^{-2i(p^2/2)t'} dt'. \quad (6)$$

The reason that Eq. (6) is called the ‘‘Wigner-distribution-like’’ function is due to that S' in Eq. (3) is a function of p while $F'(t)$ in Eq. (5) is not a function of Ω .

One interesting feature of the Wigner distribution is that it satisfies the marginal relationship. The WDL function still satisfies this condition:

$$|S_{fi}|^2 = \int f\left(t, \frac{p^2}{2}\right) dt. \quad (7)$$

The above marginal relationship can be proved by integrating Eq. (6) over t

$$\begin{aligned} \int_{-\infty}^{\infty} f\left(t, \frac{p^2}{2}\right) dt &= \int_{-\infty}^{\infty} dt \frac{1}{\pi} \int_{-\infty}^{\infty} S'^*(t+t') S'(t-t') e^{-2i(p^2/2)t'} dt' \\ &= \frac{1}{2\pi} \int_{-\infty}^{\infty} \int_{-\infty}^{\infty} S'^*(t_2) S'(t_1) e^{-i(p^2/2)(t_2-t_1)} dt_1 dt_2 \\ &= S_{fi}^* S_{fi} = |S_{fi}|^2. \end{aligned} \quad (8)$$

In the above deduction, we use the following linear transformations : $t = (t_2 + t_1)/2$, $t' = (t_2 - t_1)/2$.

After integrating Eq. (6) over $p^2/2$, one can obtain the ionization time distribution which has the form:

$$P(t) = \int f\left(t, \frac{p^2}{2}\right) d\left(\frac{p^2}{2}\right). \quad (9)$$

It is worth noting that the direction of the final electron momentum \mathbf{P} , which is dependent on the dimension of the system under study, is implicit in Eqs. (1)–(9). So far, we do not specify the system. The above formulas are general.

In this paper, we adopt the vector potential of the laser field in a general form as following:

$$\mathbf{A}(t) = -\frac{E_0}{\omega} \sin^2\left[\frac{\omega t}{n}\right] \left[\cos\frac{\theta}{2} \cos(\omega t + \varphi) \mathbf{e}_x - \sin\frac{\theta}{2} \sin(\omega t + \varphi) \mathbf{e}_y \right], \quad (10)$$

where E_0 is the peak amplitude of the laser field, φ the carrier-envelope phase and $n/2$ the number of cycles. \mathbf{e}_x and \mathbf{e}_y are the unit vectors along the x - and y -axes, respectively. $\epsilon = \cot(\theta/2)$ is the ellipticity. The major axis is y -axis.

we can set $\theta = 0$ in Eq. (10) and thus obtain the vector potential of a linearly polarized laser field as following:

$$\mathbf{A}(t) = -\frac{E_0}{\omega} \sin^2\left[\frac{\omega t}{n}\right] \cos(\omega t + \varphi) \mathbf{e}_x, \quad (11)$$

where, \mathbf{e}_x is the unit vector along the direction of the laser polarization.

In the following calculations, a two-dimensional system is employed for simplification. In the case of a two-dimensional system, for a fixed kinetic energy $p^2/2$, the electron emission angle Θ varies from 0 to 2π , where Θ is the angle between the direction of final momentum of the electron and x -axis. The WDL function can be written as:

$$f\left(t, \frac{p^2}{2}, \Theta\right) = \frac{1}{\pi} \int_{-\infty}^{\infty} S'^*(t+t', \Theta) S'(t-t', \Theta) e^{-2i(p^2/2)t'} dt'. \quad (12)$$

Further, We can obtain the ionization probability after integrating Eq. (12) over time t , kinetic energy $p^2/2$ and emission angle Θ , which is given by

$$\begin{aligned} \iiint f\left(t, \frac{p^2}{2}, \Theta\right) dt d\frac{p^2}{2} d\Theta &= \iint |S_{fi}|^2 d\frac{p^2}{2} d\Theta \\ &= \iint |S_{fi}|^2 p dp d\Theta. \end{aligned} \quad (13)$$

Obviously, the ionization probability obtained by Eq. (13) is equal to that calculated directly by the SFA theory in a two-dimensional system (Reiss, 1980).

Similarly, the time-emission angle distribution is given by

$$f'(t, \Theta) = \int f\left(t, \frac{p^2}{2}, \Theta\right) d\frac{p^2}{2}. \quad (14)$$

Then one can find that the ionization probability as functions of time and emission angle can be given by

$$P(t) = \int f'(t, \Theta) d\Theta, \quad (15)$$

and

$$W(\Theta) = \int f'(t, \Theta) dt. \quad (16)$$

From Eqs. (6), (7), and (13), it can be found that the photoelectron energy spectrum (or momentum distribution) can be

correctly obtained by integrating the WDL function over time t . Though the WDL and WD functions are not equivalent mathematically, our work shows that the WDL function can be used as a powerful tool in the study of time-related problem in the ATI as shown in the following sections.

Results and discussions

In this section, we investigate various distributions of electrons ionized from H atoms by intense laser fields with different laser parameters with the help of the WDL function. The peak intensities of all the laser pulses employed are $I = 1 \times 10^{14}$ W/cm² throughout our calculations. Atomic units (a.u.) are used unless indicated otherwise.

Results in linearly polarized laser fields

For the case of linearly polarized laser fields, we mainly focus on the electrons emitted in the directions parallel and perpendicular to the polarization, which exhibit different dynamical characteristics. Moreover, for the given emission direction, the feature is also different for electrons ionized in multi-cycle and few-cycle laser field pulses.

Results for emission in direction parallel to the laser polarization

For the electrons emitted in the polarization direction, the emission angle Θ is equal to 0 or 180° (Guo *et al.*, 2010, 2012). For multi-cycle laser pulses, all the results are almost identical for $\Theta = 0$ and $\Theta = 180^\circ$. Therefore, we only give the time-energy distribution and energy spectrum with $\Theta = 0$ for multi-cycle laser pulses.

We first show the time-energy distribution of electrons emitted along the polarization direction of the laser field with frequency $\omega = 0.182$ a.u. and pulse duration of 60 optical cycles (o.c.), which is displayed in Figure 1a. The time-energy distribution is obtained by Eq. (12) for $\Theta = 0$. Figure 1b is the energy spectrum by integrating Eq. (12) over t for $\Theta = 0$. The energy spectrum exhibits two main peaks with several subpeaks on the right side of the main peaks. The presence of the two main peaks at about $p^2/2 = 0.023$ and 0.205 a.u. is expected in the multiphoton regime since the ATI spectrum consists of discrete peaks with fixed energy interval of one photon energy.

One pronounced feature in the time-energy distribution is the crescent-like structure (e.g., the structure following the black curve in Figure 1a will be called “crescent structure” below). By comparing the time-energy distribution with the energy spectrum, the positions of crescent structures in Figure 1a correspond to peaks of the energy spectrum in Figure 1b, except that the peak at about $p^2/2 = 0.12$ a.u. which is artifact pertaining to the Wigner distribution (Cohen, 1989; Kim *et al.*, 2001). When the energy spectrum is calculated by integrating Eq. (12) over t for $\Theta = 0$, the sum of the negative values and the positive values for the peak at about $p^2/2 = 0.12$ a.u. is zero, and thus results in the disappearance of the peak at about $p^2/2 = 0.12$ a.u. in Figure 1b.

Another prominent feature is that the crescent structures corresponding to the main peaks in the energy spectrum follow the black lines shown in Figure 1a very well at a wide range of times close to the center of the laser pulse. The black lines denote the time-varying kinetic energy of electrons according to the energy conservation of the ATI process, which is given by the following formula:

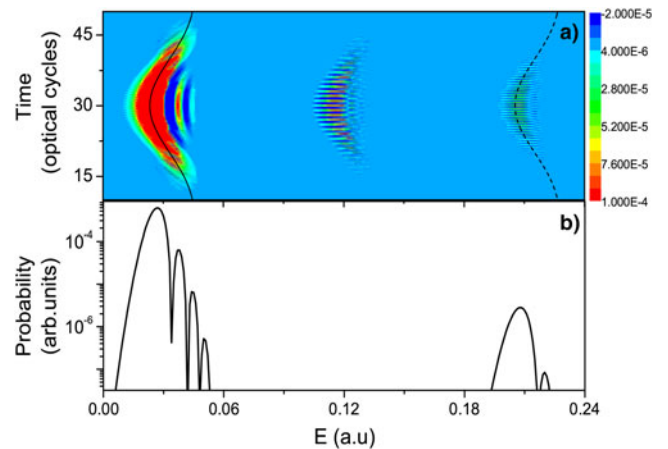


Fig. 1. Time-energy distribution (a) and energy spectrum (b) in a 60-cycle laser pulse with $\omega = 0.182$ a.u.. The time-varying final kinetic energy curves calculated by Eq. (17) correspond to the number of extra photons absorbed $S = 0$ (solid line) and $S = 1$ (dashed line), respectively. $E = p^2/2$ represents the final kinetic energy of electrons. From Guo *et al.* (2010).

$$\begin{aligned} \frac{p^2}{2} &= (N_0 + S)\omega - I_p - U_p(t) \\ &= (N_0 + S)\omega - I_p - \frac{E_0^2 \sin^4[\frac{\omega t}{n}]}{4\omega^2}. \end{aligned} \quad (17)$$

Here N_0 is the minimum number of photons needed for the ionization and S is the number of excess photons absorbed in the continuum. The two crescent structures at about $p^2/2 = 0.023$ and 0.205 a.u. in the time-energy distribution (see Figure 1a) correspond to $S = 0$ (solid line) and 1 (dashed line), respectively. It is noted that in Eq. (17), we take an envelope of the electric field approximately as $E(t) = E_0 \sin^2[\omega t/n]$. This approximation is valid when the electric-field envelope is approximately constant over one oscillation of the laser field. The validity of the above approximation reduces with the ionization time far away from the center of the pulse, which is the reason that the black lines deviate from the crescent structures at the both edges of the pulse. Clearly, one can find that the crescent structures in the time-energy distribution are not only in good agreement with peaks in the energy spectrum but consistent with the time-varying kinetic energy in the ATI process.

The origin of the subpeaks in the energy spectrum has been studied by Reed and Burnett (1991), Wickenhauser *et al.* (2006), and Della Picca *et al.* (2016). Reed and Burnett (1991) have attributed the subpeaks to the interference between the photoelectron amplitudes produced at the same laser intensity on the rising and falling edges of the pulse. Wickenhauser *et al.* (2006) have concluded that the subpeaks are caused by the changing field-dressed ionization potential during the ionization process. Della Picca *et al.* (2016) found that electron emission amplitudes produced at different times interfere with each other, which produces these subpeaks. Here, we analyze the origin of crescent substructures based on the prediction of Reed and Burnett (1991).

The energy positions of the interference minima in the time-energy distribution are given by the following formula (Reed and Burnett, 1991):

$$E_p = -I_p + N\omega - \frac{E_0^2}{4\omega^2} + \left[\frac{3\pi}{8}\right]^{2/3} \left[\frac{E_0^2}{2n^2}\right]^{1/3} (4q - 1)^{2/3}, \quad (18)$$

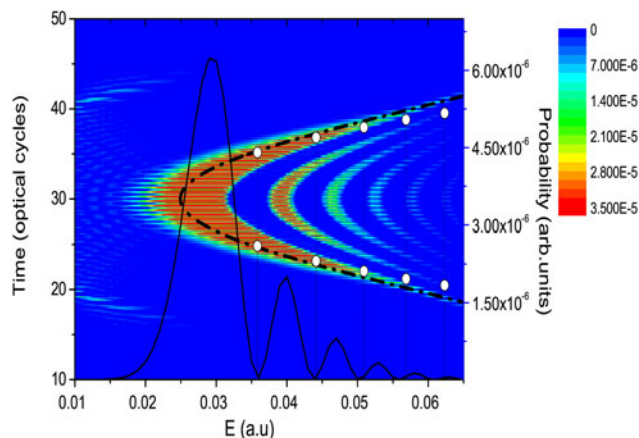


Fig. 2. Time-energy distribution with the laser parameters as those of Figure 1, except for $\omega = 0.1$ a.u.. The energy spectrum (solid line) and the time-varying kinetic energy (dashed line) are also given. The opened circles mean the points from which the electron is emitted to produce the interference minimum (see text). $E = p^2/2$ represents the final kinetic energy of electrons. From Guo *et al.* (2010).

where E_p denotes the interference minimal energy; N is the absorbed photons number and the values of parameter q are integer 1, 2, 3, The time positions of the interference minima can be obtained by assigning the energy values given by Eq. (18) to Eq. (17). Meanwhile, the following approximation is used in Eq. (17), which is

$$-U_p(t) = -\frac{E_0^2}{4\omega^2} \sin^4\left[\frac{\omega t}{n}\right] \approx -\frac{E_0^2}{4\omega^2} + \frac{E_0^2}{2n^2} \left[t - \frac{T_c}{2}\right]^2. \quad (19)$$

The opened circles in Figure 2 denote the predicted minima of the interference based on Eq. (18). Figure 2 shows the same calculations as those in Figure 1 except for $\omega = 0.1$ a.u. The positions of the interference minima agree well with minima of the energy spectrum, especially for the first pair of points. The other points slightly shift to higher energy compared with those in the energy spectrum and also deviate from the dash-dotted line. Apparently, the above approximation of Eq. (19) is more valid in the vicinity of the crest of the pulse and becomes invalid when the time varies from the center to the edges of the pulse.

Moreover, when the frequency decreases further to $\omega = 0.05691$ a.u., both the time-energy distribution and the energy spectrum become more complicated as shown in Figure 3. The structures in Figure 3 are more complex due to the appearance of more interference structures compared with those in Figures 1 and 2. Even so, the main peaks are still visible. The reason why more interference structures appear is the fact that more than one pair of ionization times satisfies Eq. (17), for a given kinetic energy. Moreover, it is noted that the interference minima given by Eq. (18), except the few points close to the main peak, are not consistent with the minima in the energy spectrum. This is because the method used to calculate the interference minima here is only valid for two saddle points, namely two ionization times. Therefore, the interference minima calculated by Eq. (18) are expected to be invalid when the number of the saddle points dominated the spectrum is four. However, the contribution of the emission of photoelectron produced at the intensity near the peak of the pulse dominates the spectrum, which results in that the interference minima positions near the main peak in the energy

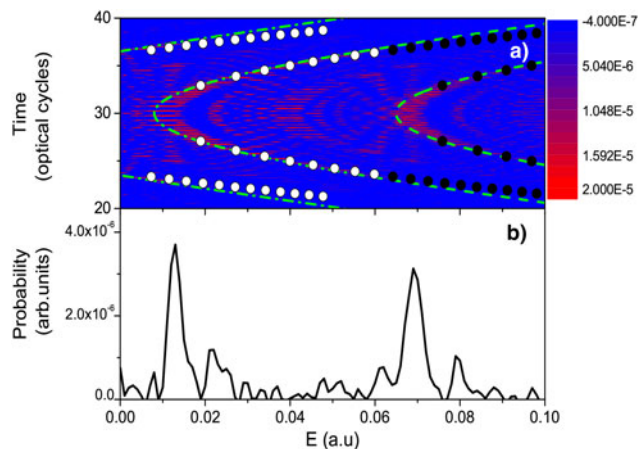


Fig. 3. Time-energy distribution (a) and energy spectrum (b). The laser parameters are the same as those of Figure 1, except $\omega = 0.05691$ a.u.. The curves calculated by Eq. (17) correspond to $S=0$ (green dash dotted line) and $S=1$ (green dashed line), respectively. The opened circles ($S=0$) and filled circles ($S=1$) represent the interference minima, respectively (see text). $E = p^2/2$ represents the final kinetic energy of electrons. From Guo *et al.* (2010).

spectrum are still in accordance with the prediction of Eq. (18) as exhibited in Figure 3.

For multi-cycle laser pulses as shown above, the structures in the time-energy distribution and energy spectrum mainly come from inter-cycle interference and are independent of the CEP and emission direction, namely $\Theta = 0$ and $\Theta = 180^\circ$ (not shown here).

When the laser pulse duration is as short as several optical cycles, the pattern of the electric field oscillation becomes very important for the ATI process. The ionization probability is dependent on the CEP and the emission direction (Milošević *et al.*, 2006). Next, we use the WDL function to show how the ionization time distribution and the time-energy distribution depend on the CEP of the laser field and the emission direction of electrons.

In Figure 4, we show the ionization time distribution of electrons emitted in two opposite directions for a four-cycle laser field with different frequencies and CEPs, which is obtained by integrating the WDL function Eq. (12) over energy $p^2/2$ for $\Theta = 0$ and $\Theta = 180^\circ$, respectively. Several features are gained from Figure 4 as the following:

- (i) Dependence of ionization time distribution on the CEP. For $\varphi = 0$, the ionization time distribution in each direction is time-symmetric with respect to the center of the electric field envelope while for $\varphi = 0.5\pi$ it becomes time-asymmetric.
- (ii) Dependence of ionization time distribution on the emission direction. For $\varphi = 0$, the pattern and the magnitude of the ionization time distribution of the electrons are clearly different in positive ($\Theta = 0$) and negative ($\Theta = 180^\circ$) directions. The ionization probability of electrons shows positive-negative (namely “left-right” in other literature) asymmetry. For $\varphi = 0.5\pi$, the magnitude of asymmetric ionization time distribution is the same in both the positive and negative directions and after integrating the ionization time distribution over time t , the yields of electrons in two opposite directions are exactly identical, which still keeps positive-negative symmetry.

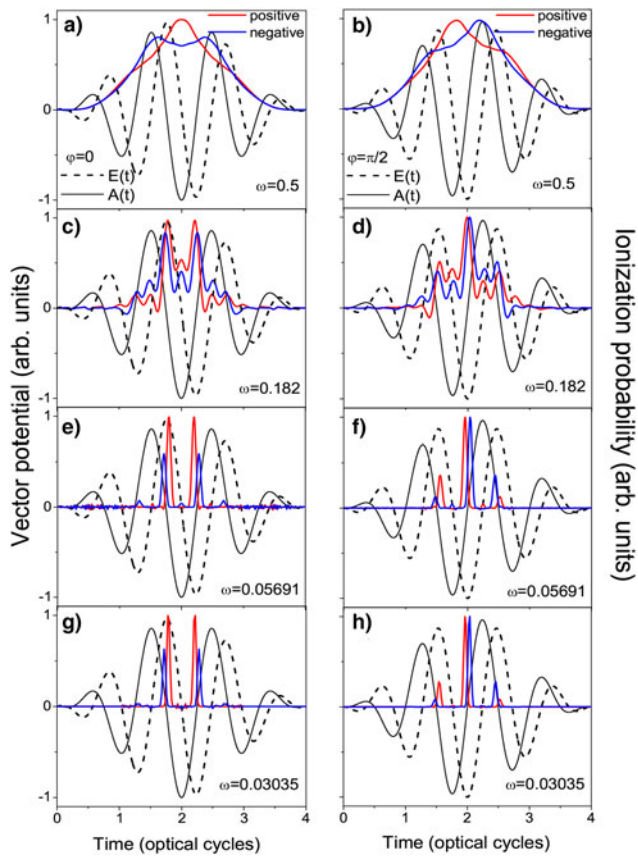


Fig. 4. Ionization time distribution of photoelectrons emitted in the positive (red solid lines) and negative (blue solid line) directions along the polarization of the laser fields with different laser frequencies and the pulse duration is 4 o.c.. The CEP $\varphi = 0$: ((a), (c), (e) and (g)); $\varphi = \pi/2$: ((b), (d), (f) and (h)). From Guo *et al.* (2012).

(iii) Dependence of ionization time distribution on the laser frequency. For the highest laser frequency $\omega = 0.5$, the ionization time distribution exhibits a rather smooth envelop, which is roughly close to the shape of the laser pulse envelop. For the laser frequency $\omega = 0.182$, the ionization probability begins to peak at times when the electric field amplitude reaches maximum (see Fig. 4c and 4d). When the laser frequency decreases further to 0.05691 and 0.03035 a.u., the ionization time distributions become more and more sensitive to the field strength as displayed in Figure 4e–h, which results in that both the positions and heights of sharp peaks are strongly dependent on the amplitude of the field maximum. This dependence of the ionization probability on the electric field exhibits the characteristic of the tunneling ionization picture.

Moreover, our calculations with the above four different laser frequencies correspond to the Keldysh parameters of 9.35, 3.4, 1.06, and 0.56, respectively. Therefore, the result in Figure 4 explicitly displays that the ionization probability becomes more and more strongly dependent on the field amplitude accompanying decrease of γ , which can be thought as a transition from the multiphoton regime to the tunneling regime. It is noteworthy that, strictly speaking, tunneling picture of ATI is only valid when the Keldysh parameter is around 1 (Keldysh, 1965; Reiss, 1980; Krainov, 1997). However, this picture (or the semiclassical

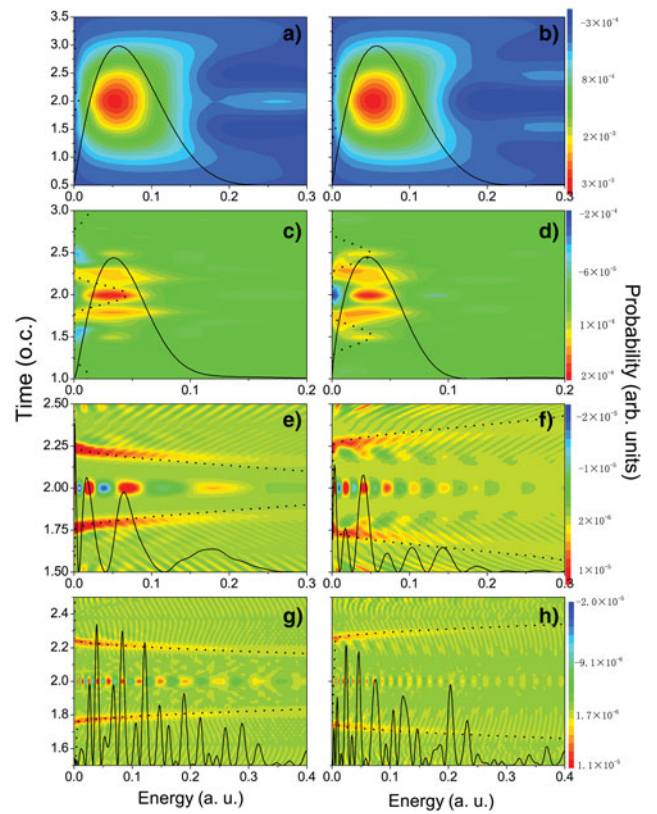


Fig. 5. Energy spectrum (solid lines) and time-energy distribution in four-cycle laser pulses with the CEP $\varphi = 0$. The laser parameters are the same as those used in Figure 4. Left and right panels are for electrons ejected in the positive and negative directions, respectively. Dotted lines denote the semiclassical curve of $p^2/2 = A^2(t)/2$. From Guo *et al.* (2012).

picture) is commonly used in atom-intense laser interactions even when $\gamma < 1$ and the theoretical results are in agreement with the experimental observations (Laroche *et al.*, 1998; Chen *et al.*, 2000). The calculations shown in Figure 4e and 4f show that the ionization process already exhibits a typical tunneling feature even when γ is around 1, despite still far from the strict theoretical requirement. Therefore, the semiclassical model is already a valid approximation when $\gamma \sim 1$.

Figure 5 gives the time-energy distributions of ATI process and the energy spectra in a four cycle laser pulse with the parameters as shown in Figure 4 and $\varphi = 0$. Both the time-energy distribution and energy spectrum exhibit dependence on the emission direction and laser frequency. For the higher frequencies $\omega = 0.5$ and 0.182 a.u., the energy spectra show one smooth peak, which have nearly no difference in the positive and negative directions (see Fig. 5a–d). Meanwhile, there are slight differences in the time-energy distributions in two opposite directions as shown in Figure 5. When $\omega = 0.05691$ and 0.03035 a.u., both the time-energy distribution and energy spectrum become strongly dependent on the emission direction. The energy spectra show complicate interference patterns, which are due to the interference between electrons emitted at different times with the same kinetic energy (which will be further analyzed below) (Reed and Burnett, 1991; Kopold *et al.*, 2002; Lindner *et al.*, 2005).

The relationship between the drift kinetic energy and ionization moment $p^2/2 = A^2(t)/2$ is also given in Figure 5 (shown by dotted line), which is based on the semiclassical picture of the

ATI ionization process that the electron's drift momentum is equal to the vector potential of the electric field with the opposite sign ($\mathbf{p} = -\mathbf{A}(t)$) in the tunneling regime. For higher laser frequencies $\omega = 0.5$ and 0.182 a.u., the drift kinetic energy in the time-energy distribution is obviously larger than the energy given by the semiclassical relationship. This is expected since in multiphoton regime, the semiclassical picture is invalid in description of the ATI process. When the frequency decreases to $\omega = 0.05691$ ($\gamma \sim 1$), the strips begin to agree qualitatively with the semiclassical relationship $p^2/2 = A^2(t)/2$ although they diverge in the higher energy especially when $E_k > 0.1$ a.u. (see Fig. 5e and 5f). The reason of the divergences may be attributed to the non-adiabatic effect since the Keldysh parameter is around 1. When $\omega = 0.03035$ a.u. ($\gamma < 1$), the relation between the ionization time and kinetic energy is consistent well with the semiclassical relationship in Figure 5g and 5h and is also in accordance with the analysis using Wigner function by Czirják *et al.* (2000) for ionization process of atoms in a static electric field.

Moreover, there are many interference structures located at about $t = 2$ o.c. in the time-energy distribution for $\omega = 0.05691$ and 0.03035 a.u. The destructive (negative distribution) and constructive (positive distribution) interferences correspond to minima and maxima in the energy spectrum (see Fig. 5e–5h), respectively. According to Lindner *et al.* (2005), the origin of the interference structures in ATI spectrum can be attributed to the double-slit interference effect. For a four-cycle pulse with sine-square envelope, the electrons ionized at times ranging from $t \sim 1.5$ to $t \sim 2.5$ o.c. (see Fig. 6) play a dominant role in the energy spectrum due to the strong dependence of the ionization probability on the electric field amplitude. Figure 6 shows the electric field and the vector potential of a four-cycle laser pulse with $\varphi = 0$. Therefore, interference structures in Figure 5e and 5g (Fig. 5f and 5h) result from the interference between the electrons emitted at two different times with the same momentum as marked by the open circles (full black circles) lying in the red (black) lines in Figure 6. From Figures 5 and 6, it can be seen that the intra-cycle interference plays an important role in the photoelectrons ionization process in few-cycle laser pulses.

The difference between the interference patterns in the negative (Fig. 5e) and positive (Fig. 5f) directions results from the different energy-dependent time interval in two different directions: the time interval decreases with increasing energy in Figure 5e (Fig. 5g) but increases with increasing energy in Figure 5f (Fig. 5h). Clearly, this interference mechanism is only applicable when the semiclassical picture of the ionization process is valid, which is only available in the tunneling regime. From Figure 5e and 5f, we can see that this mechanism is also approximately valid when $\gamma \sim 1$.

Figure 7 shows the energy spectrum and the time-energy distribution of electrons ionized by the laser pulse with the same parameters as those in Figure 5e, except for $\varphi = 0.5\pi$. The pattern of the electric field with $\varphi = 0.5\pi$ is different from the case of $\varphi = 0$. Consequently, the ionization strips appear at $t \sim 1.5, 2.0$, and 2.5 o.c., which still agree with the semiclassical relationship given by Eq. (17) (dashed line). Because of the appearance of more ionization strips in Figure 7, the interference structures become more complicated compared with the case of $\varphi = 0$ shown in Figure 5e. However, the interference mechanism appearing in Figure 7 is still the same as the case of $\varphi = 0$. It is expected that the structures located at times $t \sim 1.75$ and 2.25 o.c. in Figure 7 are similar to those in Figure 5e and 5f, respectively. In addition, the spectra of electrons emitted in both negative and positive

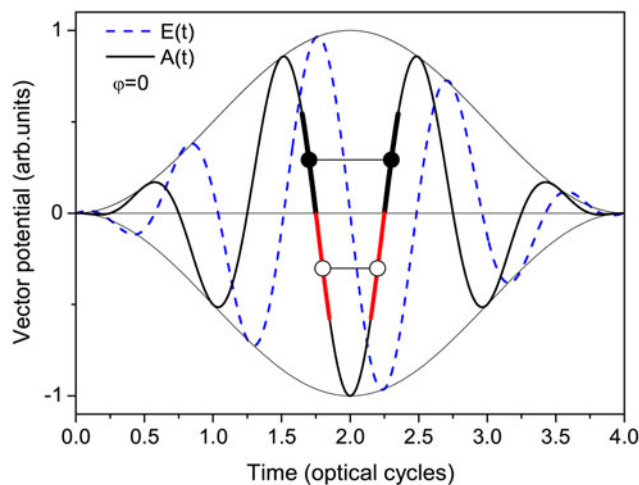


Fig. 6. Electric field and vector potential of a four-cycle laser pulse. From Guo *et al.* (2012).

directions are identical for the case of $\varphi = 0.5\pi$, consistent with the ionization probability distribution and electric field amplitude and vector potential given in Figure 4f (the electric amplitude and the vector potential satisfy $\mathbf{E}(t) = \mathbf{E}(4T - t)$ and $\mathbf{A}(t) = -\mathbf{A}(4T - t)$, respectively).

Results for emission in direction perpendicular to the laser polarization

In the transverse direction, the dynamic behavior of photoelectrons is mirror symmetric in the two opposite directions ($\Theta = 90^\circ$ and 270°) perpendicular to the polarization (Guo *et al.*, 2017). Therefore, here we only give the calculations for one fixed emission direction of $\Theta = 90^\circ$.

Figure 8a and 8b are the time-energy distribution and the energy spectrum of electrons emitted in the direction vertical to the polarization by a four-cycle laser pulse with $\varphi = 0$. The time-energy distribution (Fig. 8a) is calculated by Eq. (12) for $\Theta = 90^\circ$. After integrating the time-energy distribution over t , we obtain the energy spectrum given in Figure 8b. For comparison, we also give the absolute amplitude of the electric field as displayed in Figure 8a. From Figure 8, one can find that the ionization strips mainly appear at times $t \sim 1.75$ and $t \sim 2.25$ o.c. and the interference structure appears at time $t \sim 2.0$ o.c.. These characteristics are the same as that in the polarization direction as shown in Figure 5e and 5f. However, there are two features different from the case of the parallel direction: the ionization strips in Figure 8a are almost perpendicular to the time axis and the energy interval between constructive (or destructive) interference in the interference structures in both time-energy and energy distributions (see Fig. 8) is 2ω .

The differences mentioned above can be explained based on the semiclassical theory. According to the semiclassical picture, the electrons ejected at times when the amplitude of the laser field is maximal, regardless of the direction of the electric field vector, have only transverse momentum component (zero longitudinal momentum component since $p_{\parallel} = -A(t) = 0$). Meanwhile, the ionization probability is strongly dependent on the amplitude of the laser field. Therefore, the ionization strips appear at moments when the electric field is close to its maxima per half cycle, such as $t \sim 1.75$ and ~ 2.25 o.c.. Furthermore, with increasing final kinetic energy, the ionization moments are almost

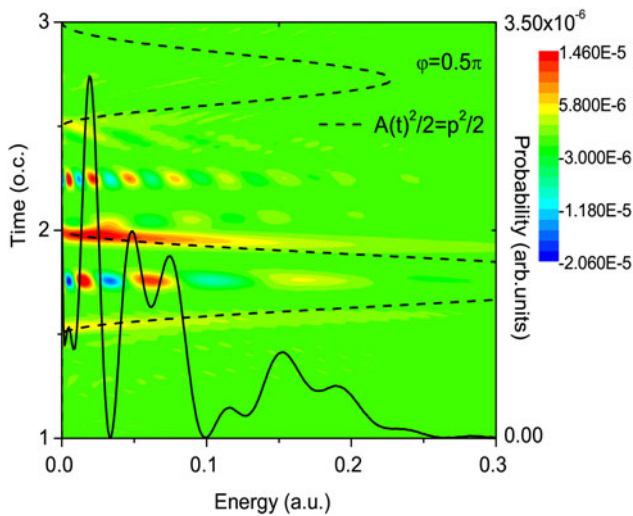


Fig. 7. Time-energy distribution and energy spectrum (solid line) in four-cycle laser pulses with parameters as those of Figure 5e, except for $\varphi = 0.5\pi$. The dashed line denotes the semiclassical curve of $p^2/2 = A^2(t)/2$. From Guo *et al.* (2012).

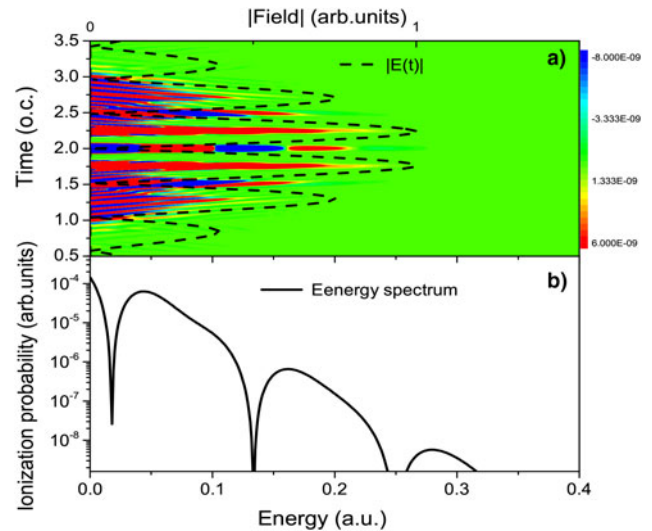


Fig. 8. Time-energy distribution (a) and energy spectrum (b) for electrons emitted in the transverse direction in a four-cycle laser pulse with the CEP $\varphi = 0$ and wavelength 800 nm. The absolute amplitude of the laser field is denoted by dashed line. Data from Guo *et al.* (2017).

constant as shown in Figure 8a, leading to the strips vertical to the time axis. The interference structure at $t \sim 2.0$ o.c. comes from the interference between electrons ionized at $t \sim 1.75$ and 2.25 o.c. with the same momentum, which has the same interference mechanism as that described in Figure 5. Due to the ionization strips located at $t \sim 1.75$ and 2.25 o.c. as shown in Figure 8a, the time interval related to interference structures is fixed and thus leads to the interference structure with fixed energy spacing. In addition, there are two additional interference structures located at $t \sim 1.5$ and 2.5 o.c. in Figure 8a, respectively. They possess the same interference mechanism as that located at $t \sim 2.0$ o.c..

Let us take the structure located at $t \sim 1.5$ o.c. as an example. It results from the interference between electrons generated at $t \sim 1.25$ and $t \sim 1.75$ o.c. It is noteworthy that the fringes of the interference at $t \sim 1.5$ and 2.5 o.c. are inclined while fringes are horizontal at $t \sim 2.0$ o.c.. The inclination (horizontal) of the fringes is owing to the fact that the electric field strengths at $t \sim 1.25$ and $t \sim 1.75$ o.c. ($t \sim 1.75$ and $t \sim 2.25$ o.c.), which are related to the interference structures, are unequal (equal) and thus lead to unequal (equal) ionization probability of electrons. Moreover, the positions of the constructive and destructive interferences in Figure 8a are in agreement with the maxima and minima in the energy spectrum displayed in Figure 8b, respectively. This indicates that the contribution of electrons emitted in the times ranging from $t \sim 1.5$ to 2.5 o.c. to spectra is dominant, while the contribution of electrons emitted in other regions, such as $t < 1.5$ o.c. and $t > 2.5$ o.c., to the final spectra is negligible due to the lower electric field strength.

The same calculations as shown in Figure 8 are performed in Figure 9 except $\varphi = 0.5\pi$. The time-energy spectrum and the energy spectrum are displayed in Figure 9a and 9b, respectively. The dashed line in Figure 9a represents the absolute amplitude of the field. Because of the change of the pattern of the laser field comparing with the case of $\varphi = 0$, three vertical ionization strips occur at $t \sim 1.5$, 2.0 and 2.5 o.c. when the laser field is close to maximum. The interference structures symmetrically appear at $t \sim 1.75$ and 2.25 o.c., respectively, of which the reason

of the inclined fringes is the same as that located at $t \sim 1.5$ o.c. in Figure 8a. Moreover, the positions of the destructive and constructive interference structures (Fig. 9a) are in good accordance with the minima and maxima in the energy spectrum (Fig. 9b), respectively. The corresponding energy interval of both two distributions are also about 2ω . Furthermore, the structure in Figure 9a is time-symmetrical, which is different from that in Figure 7 for the case of the polarization direction. This indicates that the ionization yield in the transverse direction is dependent on the magnitude but not the sign of the electric field.

Two-dimensional momentum spectra corresponding to calculations shown in Figures 8 and 9 are plotted in Figure 10a and 10b, respectively. The momentum spectra are calculated by integrating Eq. (12) over time t for the values of Θ varying from 0° to 180° . Comparing Figure 10a with Figure 10b, one can find that a clear carpet-like pattern structure is exhibited in Figure 10b as marked by a dotted box, which shows a regular grid of alternate maxima and minima interference peaks [see Korneev *et al.* (2012) for detailed descriptions]. However, the carpet-like pattern in Figure 10a is not distinct, the reason of which mainly owes to the spatial asymmetry of photoelectrons emitted, making the carpet-like structure difficult to be distinguished. Nevertheless, for a fixed direction, for example, for the emission in the transverse direction (along the dashed line in Fig. 10a), the maxima of the momentum spectrum perfectly correspond to the peaks in the energy spectrum shown in Figure 8b. The strips in Figure 10 are almost vertical, which are consistent with the pattern resulting from intra-cycle interference in Arbó *et al.* (2012).

From Figures 8 and 9, it can also be clearly seen that structures in both the time-energy distribution and the energy spectrum come from intra-cycle interference and are dependent on the CEP. In contrast to that in the polarization direction, the interference structure has equal interference interval, leading to the energy spectrum with fixed energy separations of 2ω .

Figure 11a and 11b display the time-energy distribution and the energy spectrum of electrons emitted in the laser field with the same parameters as those in Figure 9 except for the pulse

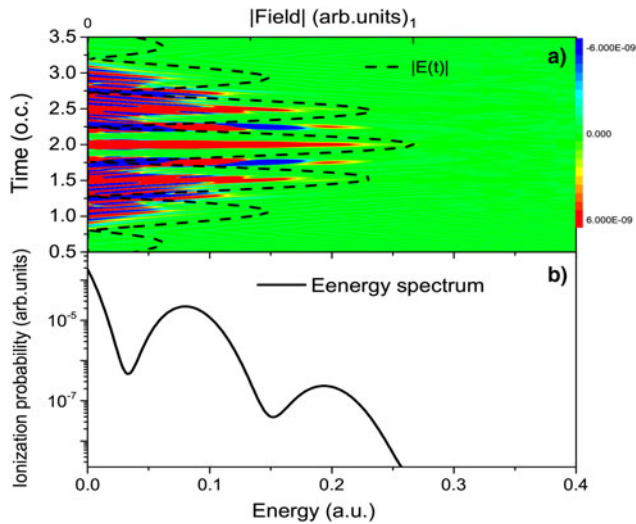


Fig. 9. Time-energy distribution (a) and energy spectrum (b) for electrons ejected in the transverse direction in a four-cycle laser pulse with the CEP $\varphi = 0.5\pi$ and wavelength 800 nm. The absolute amplitude of the laser electric field is denoted by dashed line. Date from Guo *et al.* (2017).

duration of 20 optical cycles. The energy spectrum consists of regular main peaks with series of subpeaks. In contrast to the energy spectrum in the polarization direction (see Fig. 3b), the energy interval in the energy spectrum (Fig. 11b) is 2ω , which is the same as that in the few-cycle laser pulse. The time-energy distribution (Fig. 11a) shows many crescent structures which are consistent with the time-varying kinetic energy curves (solid lines) given by Eq. (17). As displayed in Figure 11a, the crescent structure consists of the ionization strips which occur when the electric field reaches the maxima of its magnitude per half-cycle, regardless of the its direction. The origins of both the subpeaks in the energy spectrum and the crescent substructures in the time-energy distribution in Figure 11 are the same as that in the polarization direction, which are due to the interference between the electrons generated at the two same intensities on the rising and falling edges of the laser pulse.

By comparing the time-energy distribution (Fig. 11a) and the energy spectrum (Fig. 11b), one can find that the main peaks in the energy spectrum are the ATI peaks with even N while the ATI peaks with odd N become into series of subpeaks which are marked by arrows in Figure 11b. This is due to the fact that, as shown in Figure 11a, when N is an even, there are always positive interference strips between two adjacent ionization strips. Consequently, after integrating the time-energy distribution in Figure 11a over time, only ATI peak with even value of N in Figure 11b can be clearly seen because of the constructive interference. When N is odd, there are alternative positive and negative interference strips. Hence a series of subpeaks appears due to constructive and destructive interference in the integration over time. The reason of appearance of the positive (negative) interference strips described above can be further interpreted based on the saddle-point method (Korneev *et al.*, 2012). It is well-known that there are two complex saddle-point times t_1 and t_2 within one optical cycle, which satisfy $\text{Re}[\omega t_1] = 2\pi - \text{Re}[\omega t_2]$ and $\text{Im}[\omega t_1] = \text{Im}[\omega t_2]$. For electrons emitted in the transverse direction, when the ground state has an even-parity, these two quantum trajectories will interfere constructively (destructively) for even (odd) N of absorbed photons (see Korneev *et al.* (2012) for more details). Apparently, this interference

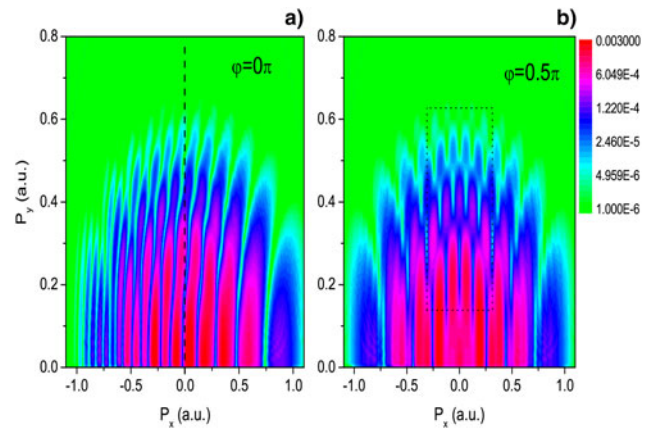


Fig. 10. Momentum distributions obtained by integrating Eq. (12) over t for the values of Θ varying from 0° to 180° with the same laser parameters as those of Figure 8 and Figure 9, respectively. From Guo *et al.* (2017).

belongs to intra-cycle interference because the interval between two ionization times is less than one cycle. From Figure 11a, the interference characteristics from inter-cycle and intra-cycle interferences can be clearly and intuitively displayed in the time-energy distribution.

Results in elliptically and circularly polarized laser fields

In order to check rigorously the principle of the “attoclock” technique, the time-emission angle distribution, ionization time distribution and angular distribution for elliptically and circularly polarized fields are calculated using both the WDL function and semiclassical theory (Guo *et al.*, 2019). By comparison between these two results, we can obtain the offset angle in the angular distributions and the offset time in the ionization time distributions. In this section, the results calculated by the WDL function are also called quantum results in order to be distinguished from the semiclassical calculations.

Results for elliptically polarized few-cycle laser pulses

We consider an elliptically polarized six-cycle laser field pulse with peak intensity of 1×10^{14} W/cm² and ellipticity $\epsilon = 0.882$ (Guo *et al.*, 2016, 2019). The semiclassical method in this section is based on the ADK model (Brabec *et al.*, 1996; Hu *et al.*, 1997; Hao *et al.*, 2011) without taking into account the ionic Coulomb potential, which corresponds to the SFA model considered in our calculation. The ionization rate of the ADK model is obtained using Eq. (21) of Krainov (1997) in which the Coulomb correction is dropped since the ionic Coulomb potential is neglected in our calculation, which has a form as follows:

$$P(t) \propto E(t)^{1.5} e^{-(2/(3E(t)))}. \quad (20)$$

The initial momentum at the tunnel exit is considered by the factor $E(t)^{-(m/2)} e^{-(p_0^2/E(t))}$ [$E(t)$ is the laser field amplitude] (Hao *et al.*, 2011). The ionization rate after considering the initial momentum distribution is obtained by multiplying Eq. (9) by the above factor. It should be noted that the factor $E(t)^{-(m/2)}$ is the normalization factor for the integral over the momentum. When only initial transversal momentum and both the initial transversal and longitudinal momenta are considered, we take $p_0 = p_{0\perp}$, $m = 1$ and $p_0^2 = p_{0\perp}^2 + p_{0\parallel}^2$, $m = 2$, respectively. Here, $p_{0\parallel}$ and $p_{0\perp}$ are the initial momentum parallel and perpendicular

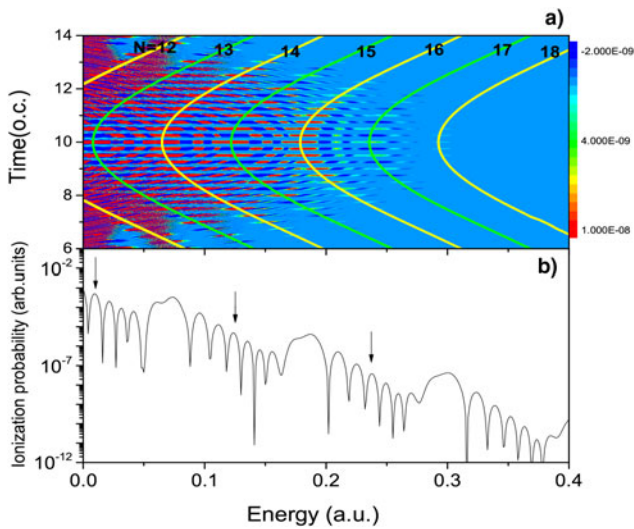


Fig. 11. Time-energy distribution (a) and energy spectrum (b) for electrons emitted in the transverse direction in a 20-cycle laser pulse with CEP $\varphi = 0.5\pi$ and $\omega = 0.05691$ a.u.. The time-dependent final kinetic energy (solid lines) are calculated by Eq. (17) for the different number N of absorbed photons as marked in the panel (a). Data from Guo *et al.* (2017).

to the direction of laser field polarization, respectively. For clarity, we label the two different semiclassical methods according to the different initial momentum adopted as ADK_{\perp} for the former and $ADK_{\perp,||}$ for the latter one.

Figure 12 shows the calculation of the time-emission angle distribution for H atoms in a six-cycle laser pulse with the CEP $\varphi = 0.5\pi$ for four different optical frequencies. The distributions in Figure 12 are obtained by Eq. (14) (see Fig. 12a, 12c, 12e, and 12g) and by semiclassical theory with $ADK_{\perp,||}$ (see Fig. 12b, 12d, 12f, and 12h), respectively. For the semiclassical calculation, all distributions with different laser frequencies look similar- two main peaks located at $[\Theta, t] \sim [0(2\pi), 2.75\text{o.c.}]$ and $[\pi, 3.25\text{ o.c.}]$ and two additional small peaks at $t \sim 2.3$ and 3.7 o.c. (not shown in Fig. 12f and 12h) which correspond to the secondary peaks of the field amplitude. This is expectable since the ionization is independent of the frequency in the quasistatic tunneling picture. In contrast, for the quantum calculation, the time-emission angle distribution shows a clear transition with decreasing laser frequency. For $\omega = 0.5\text{ a.u.}$ ($\gamma = 9.36$), one can find that the structure with a main peak at $\sim (1.5\pi, 3\text{ o.c.})$ and the other smaller peaks (Fig. 12a) is totally different from the semiclassical calculation (Fig. 12b). When the laser frequency decreases to $\omega = 0.182\text{ a.u.}$ ($\gamma = 3.4$), the distribution (Fig. 12c) is already similar to the structure of the semiclassical calculation (Fig. 12d). When the laser frequency further decreases to $\omega = 0.05691\text{ a.u.}$ ($\gamma = 1.07$) and 0.035 a.u. ($\gamma = 0.66$), the quantum results more and more mimic the semiclassical results. Therefore, Figure 12 demonstrates a transition from the multiphoton regime to the tunneling regime in the elliptically polarized laser field, which is consistent with the case of the linearly polarized laser field as shown in Figure 5.

To quantitatively investigate the accuracy of the semiclassical theory and validity of the attoclock technique, we then calculate the angular distribution $W(\Theta)$ by integrating the time-emission angle distribution over time t [namely Eq. (16)] and compare the quantum calculations with the semiclassical ones in Figure 13. All the angular distributions calculated by the semiclassical model (dashed dotted lines) show a double-peak structure, which is symmetrical with respect to the angle $\Theta = 1.5\pi$, in

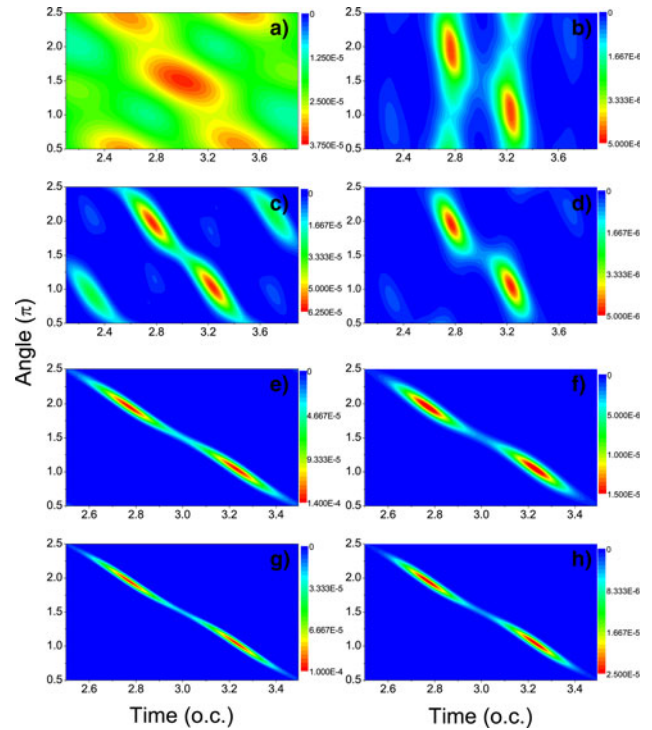


Fig. 12. Time-emission angle distributions in a six-cycle laser pulse with the CEP $\varphi = 0.5\pi$ for different laser frequencies $\omega = 0.5\text{ a.u.}$ ((a) and (b)), 0.182 a.u. ((c) and (d)), 0.05691 a.u. ((e) and (f)) and 0.03502 a.u. ((g) and (h)). Peak intensity $I = 1 \times 10^{14}$ W/cm² and the ellipticity $\epsilon = 0.882$. Quantum results: (a), (c), (e), and (g); calculations of the semiclassical theory with $ADK_{\perp,||}$: (b), (d), (f), and (h). From Guo *et al.* (2019).

accordance with those shown in Figure 12b, 12d, 12f, and 12h. However, the widths of the angular distributions become more and more broad with the increasing frequency. We also give the results obtained by ADK_{\perp} (dotted lines), which also display a symmetric double-peak. The distinct feature different from the distribution gained by $ADK_{\perp,||}$ is that the width of the angular distribution hardly depends on the frequency. By comparing between these two kinds of ADK calculations, we can infer that the initial longitudinal momentum distribution can cause broader width of the angular distribution, resulting in the difference between these two ADK calculations which becomes larger when the frequency increases.

Similar to Figure 12, the quantum calculations also clearly show a transition from the multiphoton regime to the tunneling regime with decreasing laser frequencies comparing with the semiclassical calculations. For $\omega = 0.5\text{ a.u.}$, the angular distribution shows two peaks at the emission angles of $\Theta = 0.5\pi, 1.5\pi$, which is completely different from the semiclassical calculations obtained by $ADK_{\perp,||}$ and ADK_{\perp} (see Fig. 13a). For $\omega = 0.182\text{ a.u.}$, the angular distribution in the quantum calculation also shows a double-peak pattern with peak positions close to the semiclassical distributions (see Fig. 13b). When the frequency decreases further, the quantum distribution becomes more and more close to the semiclassical calculations (see Fig. 13c and 13d), however, the widths of the quantum distributions are wider than the semiclassical ones and positions of peaks in the quantum and semiclassical calculations are still noticeable different (here, we define the difference between the peak positions in the angular distribution calculated by the quantum theory and ADK models as offset angle denoted by $\Delta\Theta$). Moreover, the effect of the initial longitudinal momentum of the photoelectron, which

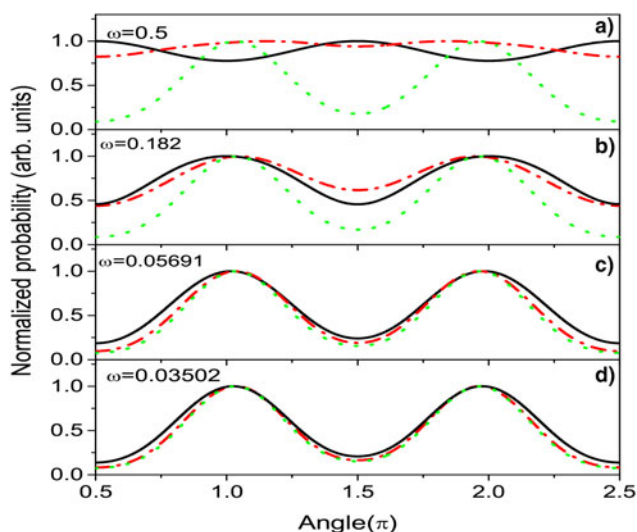


Fig. 13. Angular distributions calculated by the quantum theory (solid lines) and semiclassical theories with $ADK_{\perp,||}$ (dashed dotted lines) and ADK_{\perp} (dotted lines) for different laser frequencies with the same parameters as those in Figure 12. From Guo *et al.* (2019).

is considered as the non-adiabatic effect in the tunneling ionization process (Pfeiffer *et al.*, 2012b; Teeny *et al.*, 2016; Camus *et al.*, 2017) can also be clearly seen in Figure 13. For the lowest frequency $\omega = 0.03502$ a.u., the two different semiclassical calculations (ADK_{\perp} and $ADK_{\perp,||}$) can hardly be distinguished. For $\omega = 0.05691$ a.u., the distribution of $ADK_{\perp,||}$ becomes wider than that of ADK_{\perp} and is gradually close to the quantum distribution. The difference between two semiclassical calculations becomes larger when the frequency increases to $\omega = 0.182$ a.u., however, the distribution of $ADK_{\perp,||}$ becomes even wider than the quantum distribution. This is understandable since it is already in the multiphoton regime ($\gamma = 3.4$), the non-adiabatic effect cannot be treated properly by the semiclassical model.

Moreover, we calculate the ionization time distribution $P(t)$ by integrating the time-emission angle distribution over angle Θ and the results are depicted in Figure 14. For the semiclassical simulation, the ionization time distributions obtained by both $ADK_{\perp,||}$ and ADK_{\perp} are the same since the initial momentum distributions in two calculations are both normalized. Furthermore, it is expected that the ionization probability is only dependent on the electric field strength but independent of the laser frequency. As shown in Figure 14, the ionization time distributions obtained by the semiclassical methods (black solid line) exhibit a double-peak structure for the time range from $t = 2.5$ to 3 o.c. and are indeed independent of the laser frequency, whose peak positions correspond to the maxima of the electric field strength ($t = 2.76746$ and 3.23254 o.c.). For the quantum calculation, the distributions vary with frequency. When the laser frequency is high ($\omega = 0.5$ a.u.), the ionization time distribution displays a rather smooth and broad curve with the peak at the center of the laser pulse. In this regime, the ionization probability more likely mimics the pulse envelop rather than the electric field, which is in agreement with the case of a linearly polarized laser field as shown in Figure 4. For other lower frequencies, all ionization time distributions possess a double-peak structure and the widths of the peaks decrease with decreasing laser frequencies, becoming progressively close to the semiclassical results. However, the difference between the positions of peaks in the

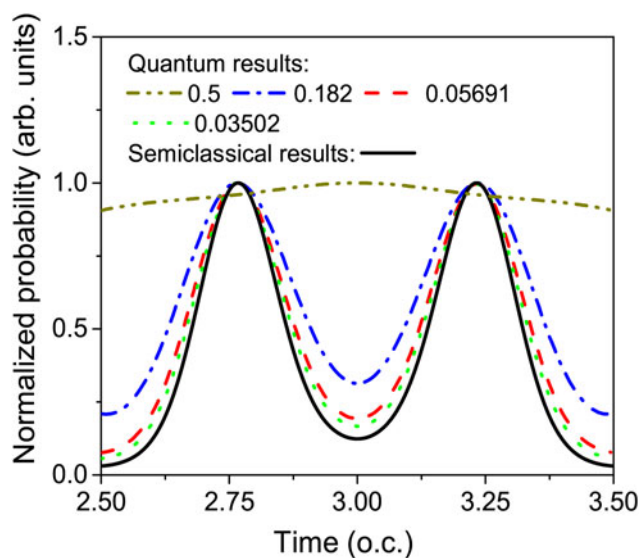


Fig. 14. Ionization time distributions calculated by the quantum theory and semiclassical theories with $ADK_{\perp,||}$ and ADK_{\perp} (solid line) for different laser frequencies with the same parameters as those in Figure 12. From Guo *et al.* (2019).

ionization time distributions calculated by the quantum method and semiclassical model still exists (for more details, see Fig. 15). We define this difference in the ionization time distribution as offset time denoted by Δt .

In addition, it is well known that for $\omega = 0.5$ a.u. which is already in the single-photon ionization regime, neither adiabatic nor non-adiabatic theories can give a proper description of the process. However, we present this calculation for a systemic investigation on the comparison between the quantum and semiclassical theories and the main conclusion of “Results in elliptically and circularly polarized laser fields” section obtained later is based on the results of lower frequencies.

Figure 15 shows the values of the offset angles (Fig. 15a) and offset times (Fig. 15b). The offset angles or times are positive and negative, corresponding to the left and right peaks exhibited in Figures 13 and 14, respectively. In order to investigate the correspondence between the offset angle and the offset time, we also give the corresponding offset angle calculated from the offset time Δt by the relation $\omega t = \Theta$. Here we define this angular offset as $\Delta\Theta_{\text{time}} = 2\pi\Delta t$ (Δt in units of o.c.). Similarly, we define the corresponding offset time transformed from the offset angle $\Delta\Theta$ in the angular distribution as Δt_{angle} ($\Delta t_{\text{angle}} = (\Delta\Theta/2\pi)$). Figure 15a shows the offset angles $\Delta\Theta$ and $\Delta\Theta_{\text{time}}$ for four different frequencies (the result of $\omega = 0.1$ a.u. is also shown here to exhibit the frequency dependence of the offset time and offset angle more clearly). One can find that the angular offset $\Delta\Theta_{\text{time}}$ is always smaller than $\Delta\Theta$ for all frequencies. Figure 15b depicts the offset time Δt and Δt_{angle} in units of attosecond (as). Some interesting features can be found in Figure 15b. The offset time hardly depends on the frequency. When the frequency decreases from 0.182 a.u. to 0.03502 a.u., the offset time Δt only changes from about 1.8 as to 1.5 as. However, the corresponding offset time Δt_{angle} varies in a much large range from 0.9 as to 26 as. This result implies that the offset angle $\Delta\Theta$ in the angular distribution does not correspond to the offset time Δt in the ionization time distribution. So the “attoclock” measurement (Eckle *et al.*, 2008b) which relies on the correspondence between the offset angle and the offset time is in principle inaccurate.

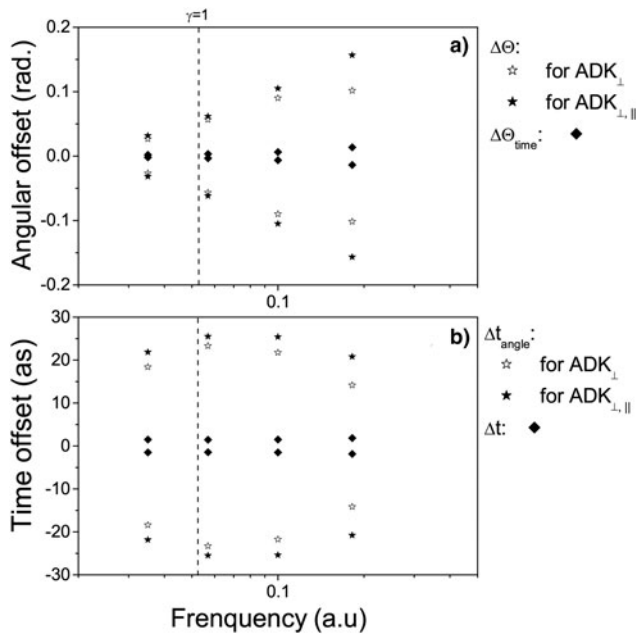


Fig. 15. The values of $\Delta\Theta$, $\Delta\Theta_{\text{time}}$ (a) and Δt , Δt_{angle} (b) obtained by different methods as shown in Figure 12 for four laser frequencies. $\Delta\Theta_{\text{time}}$ (Δt_{angle}) means the angular (temporal) offset transformed from the offset time (angle) (see text). From Guo *et al.* (2019).

It is worthwhile mentioning that for pulses with CEP $\varphi = 0.5\pi$, because the two peaks in the angular (temporal) distribution are symmetric, the absolute values of the offset angles (times) for the two peaks are equal. For other CEPs, the two peaks in the angular (ionization time) distribution become asymmetric and the absolute values of the offsets for these two peaks are not equal. Another special case is CEP $\varphi = 0$ (see Fig. 16). In this case, the maximal ionization rate occurs at the center of the laser pulse at $t = 3$ o.c. as shown in Figure 16. Figure 16a and 16b are the time-emission angle distributions calculated by the quantum theory and the semiclassical theory with ADK_{⊥,∥}, respectively. Both distributions show one main peak located at $[\Theta, t] \sim [0(2\pi), 3 \text{ o.c.}]$ and two other peaks at $t \sim 2.536$ and 3.464 o.c.. Moreover, the angular distribution and the ionization time distribution are given in Figure 16c and 16d, respectively. As displayed in Figure 16c, both angular distributions obtained by the quantum theory and semiclassical theory show two asymmetric peaks: one higher peak (namely one main peak) at emission angle $\Theta = 2\pi$ and one lower peak at emission angle $\Theta = \pi(3\pi)$. The peak positions of the two peaks calculated by these two methods coincide with each other, which means that the offset angles for the both higher peak and lower peak are all zero $\Delta\Theta = 0$. However, the ionization time distributions shows a three-peak structure. For the highest peak at $t = 3$ o.c. which corresponds to the maximal field of the laser pulse, the offset time Δt is zero. For the another two peaks on the both sides of the highest peak, these peaks are symmetric with respect to the center of the pulse $t = 3$ o.c. and the absolute values of the offset time are equal $|\Delta t| = 0.004$ o.c. (see Fig. 16d).

Results for circularly polarized few-cycle laser pulses

The calculations for circularly polarized laser pulses are shown in Figure 17. There is only one peak in both the angular and ionization time distributions and the peak positions both coincide with the ADK (solid line) calculations, in agreement with the results of

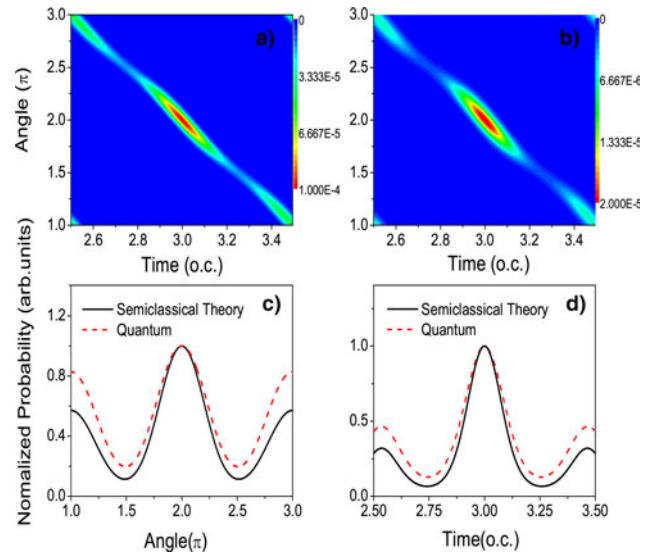


Fig. 16. Time-angle distributions calculated by the quantum theory (a) and the semiclassical theory with ADK_{⊥,∥} (b) for $\omega = 0.05691$ a.u. Angular distribution (c) and ionization time distribution (d) obtained by the quantum and semiclassical methods. The parameters are the same as those of Figure 13c except CEP $\varphi = 0$. From Guo *et al.* (2019).

Torlina *et al.* (2015). In this case, for any value of the CEP, the maximum of the laser field corresponds to the center of the envelope. Therefore both the angular and ionization time distributions also show one peak with $\Delta t = 0$ and $\Delta\Theta = 0$, which is independent of the calculation method.

Discussion

In the WDL function, to obtain the ionization time distribution in the quantum theory, correlation effect must be taken into account. The ionization probability at moment t is integration of the correlation between the ionization at $t + t'$ and $t - t'$ where t' goes over the whole laser pulse, which means that the quantum process is temporally nonlocalized. In contrast, the ionization process in the semiclassical picture is temporally localized, viz., ionization at one moment is independent of ionization at other moment. Therefore, the semiclassical theory is an approximate description of the photoionization process and, as shown by our calculation, is usually not quantitatively consistent with the quantum calculation. The coincidence of the two calculations in some specific cases is actually accidental and can be attributed to the time-reverse invariant symmetry of the laser field. For a laser pulse with CEP $\varphi = 0$ or a circularly polarized laser pulse with any CEP, the laser field possesses time-reverse invariant symmetry with maximum at the center of the laser pulse as shown in Figure 18. Therefore, the ionization time and angular distributions are symmetrical and the positions of the peaks (the higher peak in the elliptically polarized case with $\varphi = 0$), which are generated at the maximum of the laser field, are independent of the calculation method. For CEP $\varphi = 0.5\pi$, though the laser field is also time-reverse invariant, this symmetry cannot ensure the coincidence between the peaks of different calculation methods but guarantee that the offsets of the two symmetrical peaks in both the ionization time and angular distributions are symmetrical (positive and negative but the absolute values are the same, see Figs. 13–15). Moreover, as mentioned before, the lower peaks in the angular distribution for two calculations also coincide with

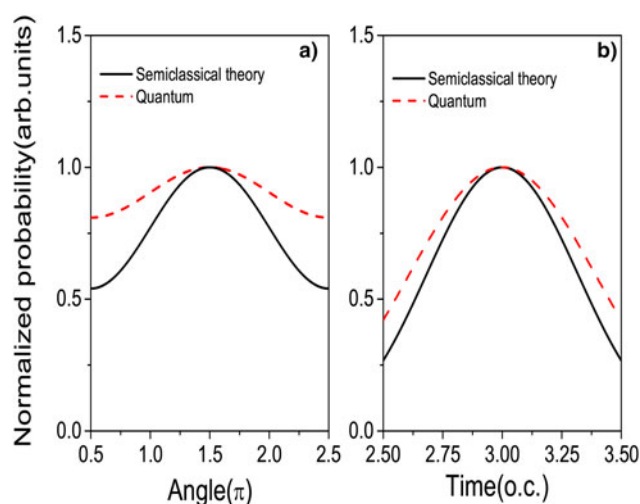


Fig. 17. Angular (a) and temporal (b) distributions obtained by the quantum and semiclassical methods for a circularly polarized laser pulse. The parameters are the same as those of Figure 16 except CEP $\varphi = 0.5\pi$. From Guo *et al.* (2019).

each other in the case of $\varphi = 0$ (see Fig. 16c). This is because that the lower peak in the angular distribution is actually composed of two halves symmetrical with respect to $\Theta = \pi$ which are generated by two symmetrical peaks with respect to $t = 3$ o.c. in the ionization time distribution (see Fig. 16d) and this symmetry is independent of the calculation method. Moreover, our analysis indicates that neither the offset time nor the offset angle in the elliptically polarized laser field can be interpreted as the tunneling time delay. These offsets, together with the widths of the peaks in the distributions, however, could be taken as effective measures for the validity of the semiclassical theory in description of the ionization process in the laser fields.

Conclusions and outlook

In conclusion, we use WDL function to study ATI of atom in laser fields with different polarization and pulse durations. We calculate the time-energy distribution and the ionization time distribution for the linearly polarized laser field and the time-emission angle, the ionization time, and the angular distributions for elliptically polarized few-cycle laser fields. For linearly polarized multi-cycle laser pulses, the time-energy distribution shows crescent structures, the positions of which can be well predicted by energy conservation equation. The sub-crescent structures in the time-energy distribution correspond to the subpeaks in the ATI energy spectrum, which can be attributed to the interference between the electrons ionized on the rising and falling edges of the laser pulse. For linearly polarized few-cycle laser pulses, both the time-energy and the ionization time distributions of electrons emitted in the direction of the polarization exhibit a transition of ionization process from the multiphoton regime to the tunnel regime with decreasing frequencies (namely decreasing Keldysh parameter). Accompanying this transition, the semiclassical picture of the ATI process, based on a correspondence between the final drift momentum and the ionization moment, becomes progressively valid and is consistent with the time-energy distribution in the tunneling regime. Meanwhile, the photoelectron energy spectrum is more and more dependent on emission direction of the photoelectron and CEP of the laser field. Furthermore, The time-energy distributions of electrons emitted

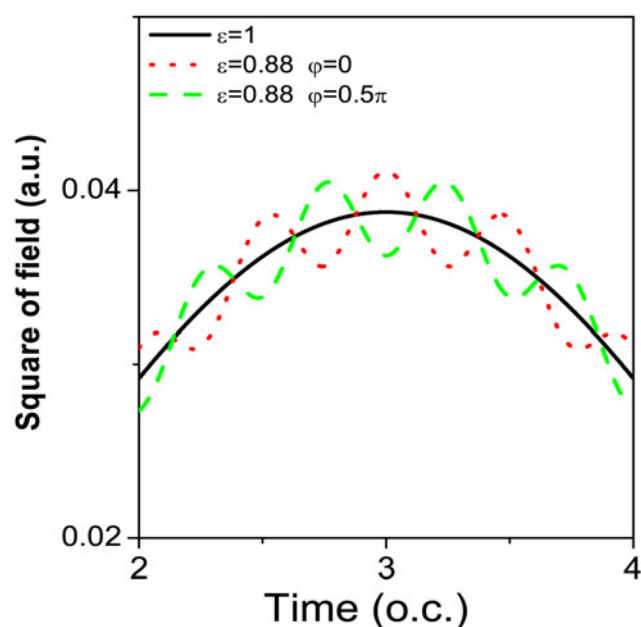


Fig. 18. Square of electric field of elliptically and circularly polarized laser pulses. From Guo *et al.* (2019).

in the direction perpendicular to the polarization show distinct interference structures with regular energy separation of 2ω , which are consistent with the corresponding energy spectra. These interference structures can be attributed to the intra-cycle interference between electrons ejected at times when the laser field is close to its extreme, which is the reason that results in the carpet-like pattern in the momentum spectrum.

For elliptically polarized few-cycle laser pulses, the time-emission angle distribution, the angular distribution and the ionization time distribution of atoms are calculated by using both WDL function and semiclassical theory. All distributions gained by WDL function are usually not in quantitative agreement with the semiclassical model calculations except in some specific cases for example, the cases of an elliptically polarized pulse with $\varphi = 0$ and a circularly polarized pulse with any value of φ . Moreover, we find that the offset angles are generally not in consistent with the offset times, indicating that the attosecond angular streaking technique is in principle inaccurate. Our result clearly shows the applicability and limit of the technique, which is important for interpretation and understanding of relevant experimental and theoretical results.

As shown above, the WDL function provides a useful tool for analysis of time-related problems in atomic photoionization process in intense laser fields. Next, it can be extended to study relevant processes in molecules, which possess more complexities, for example, alignment, multi-center, and multi-orbit effects and so on. Furthermore, the extension to include rescattering is another interesting and important work to be addressed. Taking into account the second term, that is, the rescattering term, in the S-matrix expansion, the WDL function can be applied to investigate time-related problems in the rescattering process like plateau and cutoff in high energy ATI, resonance-like enhancement structure and low-energy structure and so on.

Acknowledgements. This work was partially supported by the National Key program for S&T Research and Development (No. 2016YFA0401100), NNSFC (No. 11774361, 11775286 and 11425414) and the Open Fund of the State Key Laboratory of High Field Laser Physics (SIOM).

References

- Agostini P, Fabre F, Mainfray G and Petite G (1979) Free-free transitions following six-photon ionization of xenon atoms. *Physical Review Letters* **42**, 1127.
- Arbó DG, Ishikawa KL, Schiessl K, Persson E and Burgdörfer J (2010) Intracycle and intercycle interferences in above-threshold ionization: The time grating. *Physical Review A* **81**, 021403(R).
- Arbó DG, Ishikawa KL, Persson E and Burgdörfer J (2012) Doubly differential diffraction at a time grating in above-threshold ionization: Intracycle and intercycle interferences. *Nuclear Instruments and Methods in Physics Research B* **279**, 24.
- Barth I and Smirnova O (2011) Nonadiabatic tunneling in circularly polarized laser fields: Physical picture and calculations. *Physical Review A* **84**, 063415.
- Becker W, Grasbon F, Kopold R, Milošević DB and Paulus GG (2002) Above-threshold ionization: From classical features to quantum effects. *Advances In Atomic, Molecular, and Optical Physics* **48**, 35–98.
- Boge R, Cirelli C, Landsman AS, Heuser S, Ludwig A, Maurer J, Weger M, Gallmann L and Keller U (2013) Probing nonadiabatic effects in strong-field tunnel ionization. *Physical Review Letters* **111**, 103003.
- Brabec T, Ivanov MY and Corkum PB (1996) Coulomb focusing in intense field atomic processes. *Physical Review A* **54**, R2551–R2554.
- Camus N, Yakaboylu E, Fechner L, Klaiber M, Laux M, Mi Y, Hatsagortsyan KZ, Pfeifer T, Keitel CH and Moshhammer R (2017) Experimental evidence for quantum tunneling time. *Physical Review Letters* **119**, 023201.
- Chen J, Liu J and Chen SG (2000) Rescattering effect on phase-dependent ionization of atoms in two-color intense fields. *Physical Review A* **61**, 033402.
- Chen J, Chu SI and Liu J (2006) Time-frequency analysis of molecular high-harmonic generation spectrum by means of wavelet transform and Wigner distribution techniques. *Journal of Physics B Atomic Molecular and Optical Physics* **39**, 4747.
- Cohen L (1989) Time-Frequency Distributions a Review. *Proceedings of the IEEE* **77**, 941–981.
- Corkum PB (1993) Plasma perspective on strong-field multiphoton ionization. *Physical Review Letters* **71**, 1994–1997.
- Czirják A, Kopold R, Becker W, Kleber M and Schleich WP (2000) The Wigner function for tunneling in a uniform static electric field. *Optics Communications* **179**, 29.
- Della Picca R, Gramajo AA, Garibotti CR, López SD and Arbó DG (2016) Nonconstant ponderomotive energy in above-threshold ionization by intense short laser pulses. *Physical Review A* **93**, 023419.
- Eckle P, Smolarski M, Schlup P, Biegert J, Staudte A and Schöffler M (2008a) Attosecond angular streaking. *Nature Physics* **4**, 565–570.
- Eckle P, Pfeiffer AN, Cirelli C, Staudte A and Dörner R (2008b) Attosecond ionization and tunneling delay time measurements in helium. *Science* **322**, 1525–1529.
- Eslami E and Basereh K (2013) Effects of plasma and ultrashort laser pulse on residual electron energy in optical-field-ionized oxygen plasma. *Laser And Particle Beams* **31**, 187–193.
- Faisal FMH (1973) Multiple absorption of laser photons by atoms. *Journal of Physics B Atomic Molecular and Optical Physics* **6**, L89.
- Garg JB, Rainwater J and Havens WW (1965) Neutron resonance spectroscopy. V. Nb Ag I and Cs. *Physical Review* **137**, B547.
- Guo L, Han SS and Chen J (2010) Time-energy analysis of above-threshold ionization. *Optics Express* **18**, 1240–1248.
- Guo L, Han SS and Chen J (2012) Time-energy analysis of above-threshold ionization in few-cycle laser pulses. *Physical Review A* **86**, 053409.
- Guo L, Han SS and Chen J (2016) Study of above-threshold ionization by “Wigner-distribution-like function”. *Acta Physica Sinica* **65**, 223203.
- Guo L, Han SS, Hu SL and Chen J (2017) Time-energy analysis of above-threshold ionization in the transverse direction of the linearly polarized laser pulses. *Journal of Physics B Atomic Molecular and Optical Physics* **50**, 125006.
- Guo L, Hu SL, Liu MQ, Shu Z, Liu XW, Li J, Yang WF, Lu RH, Han SS and Chen J (2019) Accuracy of the semiclassical picture of photoionization in intense laser fields. Available at <https://arxiv.org/abs/1905.00213>.
- Hao XL, Li WD, Liu J and Chen J (2011) Effect of the electron initial longitudinal velocity on the nonsequential double-ionization process. *Physical Review A* **83**, 053422.
- Heuvel HB, van Linden van den and Muller HG (1988) Limiting cases of excess-photon ionization. In Smith SJ and Knight PL (eds), *Multiphoton Processes*. Cambridge: Cambridge University Press, pp. 25–34.
- Hofmann C, Landsman AS, Cirelli C, Pfeiffer AN and Keller U (2013) Comparison of different approaches to the longitudinal momentum spread after tunnel ionization. *Journal of Physics B Atomic Molecular and Optical Physics* **46**, 125601.
- Hofmann C, Zimmermann T, Zielinski A and Landsman AS (2016) Non-adiabatic imprints on the electron wave packet in strong field ionization with circular polarization. *New Journal of Physics* **18**, 043011.
- Hu B, Liu J and Chen SG (1997) Plateau in above-threshold-ionization spectra and chaotic behavior in rescattering processes. *Physical Letter A* **236**, 533–542.
- Ivanov IA and Kheifets AS (2014) Strong-field ionization of He by elliptically polarized light in attoclock configuration. *Physical Review A* **89**, 021402.
- Keldysh LV (1965) Ionization in the field of a strong electromagnetic wave. *Journal of Experimental and Theoretical Physics* **20**, 1307.
- Kim JH, Lee DG, Shin HJ and Nam CH (2001) Wigner time-frequency distribution of high-order harmonics. *Physical Review A* **63**, 063403.
- Klaiber M, Hatsagortsyan Z and Keitel CH (2015) Tunneling dynamics in multiphoton ionization and attoclock calibration. *Physical Review Letters* **114**, 83001.
- Kopold R, Becker W, Kleber M and Paulus GG (2002) Channel-closing effects in high-order above-threshold ionization and high-order harmonic generation. *Journal of Physics B Atomic Molecular and Optical Physics* **35**, 217.
- Korneev PA, Popruzhenko SV, Goreslavski SP, Yan TM and Bauer D (2012) Interference Carpets in Above-threshold ionization: from the Coulomb-free to the Coulomb-dominated regime. *Physical Review Letters* **108**, 223601.
- Krainov VP (1997) Ionization rates and energy and angular distributions at the barrier-suppression ionization of complex atoms and atomic ions. *Journal of the Optical Society of America B* **14**, 425.
- Krausz F and Ivanov M (2009) Attosecond physics. *Reviews of Modern Physics* **81**, 163–234.
- Kruit P and Read FH (1983) Magnetic-field parallelizer for 2-pi electron spectrometer and electron-image magnifier. *Journal of Physics E: Scientific Instruments* **16**, 313–324.
- Landsman AS, Weger M, Maurer J, Boge R, Ludwig A, Heuser S, Cirelli C, Gallmann L and Keller U (2014) Ultrafast resolution of tunneling delay time. *Optica* **1**, 343–349.
- Laroche SFJ, Talebpoury A and Chin SL (1998) Coulomb effect in multiphoton ionization of rare-gas atoms. *Journal of Physics B Atomic Molecular and Optical Physics* **31**, 1215.
- Lindner F, Schätzel MG, Walther H, Baltuška A, Goulielmakis E, Krausz F, Milošević DB, Bauer D, Becker W and Paulus GG (2005) Attosecond double-slit experiment. *Physical Review Letters* **95**, 040401.
- Lompré LA, L’Huillier A, Mainfray G and Manus C (1985) Laser-intensity effects in the energy-distributions of electrons produced in multiphoton ionization of rare-gases. *Journal of the Optical Society of America B* **xtbf2**, 1906.
- Milošević DB, Paulus GG, Bauer D and Becker W (2006) Above-threshold ionization by few-cycle pulses. *Journal of Physics B Atomic Molecular and Optical Physics* **39**, R203–R262.
- Offenberger AA, Blyth W, Preston SG, Wark JS, Key MH, Dangor AE, Modena A, Najmudin Z, Djaoui A and Key MH (1995) Optical ionization and heating of gases by intense picosecond KrF laser radiation. *Laser And Particle Beams* **13**, 19–31.
- Pfeiffer AN, Cirelli C, Smolarski M, Dörner R and Keller U (2011) Timing the release in sequential double ionization. *Nature Physics* **7**, 428–433.
- Pfeiffer AN, Cirelli C, Smolarski M, Dimitrovski D, Abu-samhaet M, Madsen LB and Keller U (2012a) Attoclock reveals natural coordinates of the laser-induced tunnelling current flow in atoms. *Nature Physics* **8**, 76–80.
- Pfeiffer AN, Cirelli C, Landsman AS, Smolarski M, Dimitrovski D, Madsen LB and Keller U (2012b) Probing the longitudinal momentum spread of the electron wave packet at the tunnel exit. *Physical Review Letters* **109**, 083002.

- Reed VC and Burnett K** (1991) Role of resonances and quantum-mechanical interference in the generation of above-threshold-ionization spectra. *Physical Review A* **43**, 6217–6226.
- Reiss HR** (1980) Effect of an intense electromagnetic field on a weakly bound system. *Physical Review A* **22**, 1786.
- Teeny N, Yakaboylu E, Bauke H and Keitel CH** (2016) Ionization time and exit momentum in strong-field tunnel ionization. *Physical Review Letters* **116**, 063003.
- Torlina L, Morales F, Kaushal J, Ivanov I, Kheifets A, Zielinski A, Scrinzi A, GeertMuller H, Sukiasyan S, Ivanov M and Smirnova L O** (2015) Interpreting attoclock measurements of tunnelling times. *Nature Physics* **11**, 503–508.
- Wang CL, Lai XY, Hu ZL, Chen YJ, Quan W, Kang HP, Gong C and Liu XJ** (2014) Strong-field atomic ionization in elliptically polarized laser fields. *Physical Review A* **90**, 013422.
- Wickenhauser M, Tong XM and Lin CD** (2006) Laser-induced substructures in above-threshold-ionization spectra from intense few-cycle laser pulses. *Physical Review A* **73**, 011401(R): 1–4.
- Wu J, Schmidt LPH, Kunitski M, Meckel M, Voss S, Sann H, Kim H, Jahnke T, Czasch A and Dörner R** (2012) Multiorbital tunneling ionization of the CO molecule. *Physical Review Letters* **108**, 183001.
- Yudin GL and Ivanov MY** (2001) Nonadiabatic tunnel ionization: Looking inside a laser cycle. *Physical Review A* **64**, 013409.